Journal of
Materials Chemistry C

Accepted Manuscript

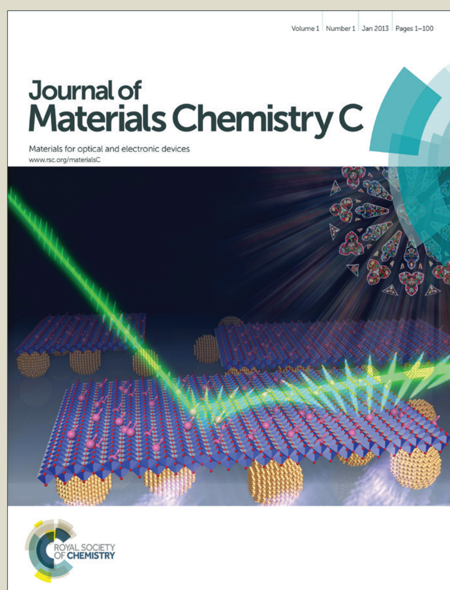

This is an *Accepted Manuscript*, which has been through the Royal Society of Chemistry peer review process and has been accepted for publication.

Accepted Manuscripts are published online shortly after acceptance, before technical editing, formatting and proof reading. Using this free service, authors can make their results available to the community, in citable form, before we publish the edited article. We will replace this *Accepted Manuscript* with the edited and formatted *Advance Article* as soon as it is available.

You can find more information about *Accepted Manuscripts* in the Information for Authors.

Please note that technical editing may introduce minor changes to the text and/or graphics, which may alter content. The journal's standard Terms & Conditions and the Ethical guidelines still apply. In no event shall the Royal Society of Chemistry be held responsible for any errors or omissions in this *Accepted Manuscript* or any consequences arising from the use of any information it contains.

ROYAL SOCIETY OF CHEMISTRY

www.rsc.org/materialsC

Please do not adjust margins

Journal of Materials Chemistry C

ARTICLE

How does the multiple constituent affect the carrier generation and charge transport in multicomponent TCOs of In-Zn-Sn Oxide

Received 00th January 20xx,
Accepted 00th January 20xx

DOI: 10.1039/x0xx00000x

www.rsc.org/

Ying-Bo Lu,* T. L. Yang, Z. C. Ling, Wei-Yan Cong, Peng Zhang, Y. H. Li and Y. Q. Xin

The main purpose of this work is to make clear that in the new synthesized multicomponent materials IZTO, namely, Sn/Zn cosubstituted In_2O_3, how can these cosubsituted dopants interact with each other and affect the electronic properties. We carry out series of systematic Density Functional Theory calculations. Compared with ITO materials, the existence of Zn^{2+} in IZTO is important to the control of the electronic properties. Although there is large lattice distortion in the local structure around Zn^{2+} due to Jahn-Teller effect, it releases distortions induced by other defects and thusthen reduces the formation energy of cosubstitution of Zn/Sn impurity pair in In_2O_3. V_O defect prefers to form in ZnO_6 octahedron for the breaking of Zn-O bond is easier than Sn-O bond, which generates free electrons. In all IZTO configurations with and without defects, the bottom of conduction bands are comprised mainly of cation-*s* and O-*p* orbitals, which constructs a three dimensional network for charge transport. Bandstructure renormalization effect conducted by Zn atom narrows the band gap. The existence of Zn atom, on the one hand weakens the spatial localization and orbital localization effects induced by defects and on the other hand strengthens the charge transport ability. These results indicate that the multicomponent semiconductor IZTO is an excellent candidate for the low indium content TCOs. Our work is useful to the control of the physical properties of IZTO experimentally, and is also helpful in understanding other multicomponent TCOs materials.

Introduction

The transparent conductive oxides (TCOs) possess two properties that are typically mutually exclusive of one another: high electrical conductivity and optical transparency, making them widely applied in optoelectronics.[1] A number of TCOs materials are based on indium oxide (In_2O_3) doped with Zn, Cd, Sn, and Ga etc.. Tin-doped In_2O_3 (ITO) is the current choice of TCOs, but some drawbacks, for example, the rather high price of indium, relative low work function, the inhomogeneity of surface properties, etc., [2-4] hinder ITO in the large-scale production of next generation flat panel display and photovoltaic technologies. The search for previously unidentified and less expensive conductive materials with good chemical stability, high transparency and electric conductivity is crucial for photovoltaic technologies.

Intensive efforts are then made to discover low indium (In) content alternative TCOs with excellent electrical and optical properties. In essence, enhanced performance must be achieved by increasing the carrier mobility, i.e., decreasing the effective mass, rather than increasing the carrier density due to the far-infrared absorption.[4-6] Making TCOs with high mobility basically depends on several principles: firstly, as many component oxides need to be used; secondly, the structures of these component oxides are quite distinctive. These two principles give birth to the third principle, also the most important one: *s*-orbitals of metal ions must be the main component of the bottom of conduction band (CB).[7, 8] Therefore, multicomponent of binary or ternary oxides based on heavy metal oxides with $(n-1)d^{10}ns^0$ electronic configuration have been assessed as replacements for ITO recently, for example, AZO, GZO, IZO,[9] TZO,[10] IGZO,[11-14] In-Mg-Sn-O, Zn-Cd-O, In-Cd-O and Cd-In-Sn-O, etc.. [15-20] These materials have unusual high electron mobility over 10 ($cm^2V^{-1}s^{-1}$).[21] As compounds with large *d* character at the conduction band minimum (CBM) have much larger electronic effective mass, the filled *d*-shell in these compounds precludes the possibility of *d-d* interband transitions, and does not typically take part in TCOs bonding process. Meanwhile, the bonding interaction is primarily composed of spatial expanding metal n*s* orbitals with isotropic shape, where the direct overlap among the neighboring metal n*s* orbitals is possible,[11] which is beneficial to generate high mobility. Based on these reasons, the lowest effective mass chemistries are correlated with Zn^{2+}, Ga^{3+}, Ge^{4+}, Cd^{2+}, In^{3+} and Sn^{4+}, etc., which contribute strong *s* character in CBM.[6, 12, 22]

Therefore, careful engineering of materials made up of these elements with conduction *s* orbitals[14, 23] can render them useful materials for TCOs applications. Among them, the extended bixbyite solid solution In-Zn-Sn-O (IZTO) system, i.e., cosubstitution of In by equal amounts of Zn and Sn, is particularly interesting.[3, 9, 23-32] The constituent compound of IZTO, namely, ZnO and SnO_2 have already been estimated to have low solubility in In_2O_3 isolatedly, for example, 6 cation% for SnO_2 and <1 wt.% for ZnO, respectively.[33] However, Palmer et al. discovered that when ZnO and SnO_2 are

[a] School of Space Science and Physics, Shandong University, Weihai 264209, P.R. China. E-mail: lyb@sdu.edu.cn

Please do not adjust margins

Journal of Materials Chemistry C Accepted Manuscript

Please do not adjust margins

cosubstitued into In_2O_3, their solubility increases dramatically, and the In content can be as low as 60 cation%, resulting from the isovalent substitution of a Sn^{4+} and a Zn^{2+} for a pair of In^{3+} cations.[15, 34-36] Accordingly, electrical and optical properties of IZTO materials have been reported to be tunable via the chemical composition adjustment. The best reported values for the resistivity of IZTO ranged from $3\sim8\times10^{-4}$ Ω·cm.[26, 33, 36-41] All IZTO films show optical transmittance over 80% in the visible region, indicating the comparable to or greater optoelectronic properties than that of the commercial ITO.[25, 26, 40-44] The band gap can be adjusted by the controlling of ZnO and SnO_2 content.[45] In addition, IZTO electrodes show superior stability against PEDOT:PSS and high work function etc.[2, 3] Hence, IZTO material is the potential replacement of ITO owing to its competitive conductivity and transparency with lower indium content.[46]

As the Sn/Zn cosubstitution brings so many physical property changes for In_2O_3 materials, the conduction mechanism of IZTO materials has been studied intensively. Pure In_2O_3 is degenerate n-type semiconductor due to the oxygen vacancies (V_O). By the substitution of Sn^{4+} on In^{3+}, Sn_{In} defect donates one free electron and behaves as V_O-like defects.[47] When IZTO is prepared with slight Sn excess,[35, 37] the conductivity is 2500S/cm, nearing that of ITO.[10, 36] While Zn^{2+} substitution of In^{3+} creates hole and decreases the free electron density.[25] Nevertheless, Zn^{2+} ions combine preferentially with oxygen atoms, leading to the production of V_O in In_2O_3,[48] which increases the carrier density in IZTO materials consequently.

Annealing of IZTO in reduction environment yields less than a 10% conduction increase,[37, 40, 45, 49] while annealing in oxidation atmosphere results in the decrease of the conductivity, the concentration of carriers and the optical band gap.[32, 34, 35, 40] Harvey et al. suggested that the Frank–Köstlin (F-K) defect, $2Sn_{In}•O_i$, may appears in IZTO. [33, 49] Addition or removal of oxygen from the neutral $2Sn_{In}•O_i$ cluster results in large changes in the effective donor concentration. It has been proposed that not all Zn cations contribute holes, but rather some form neutral associates with oxygen vacancies, such as $2Zn_{In}•V_O$ complex. Upon oxidation, some of these complexes may be dissociated, allowing zinc recovers to an acceptor and decreases the carrier concentration.[34]

Besides the carrier generation, there is another key factor in determining the electronic and optical properties, i.e., the bandstructure. The optical band gaps of TCOs are determined by both the Moss-Burstein effect and bandstructure renormalization effect arising from many-body interactions.[13, 50] The position, the dispersion and character of the bottom of CB are the most important features of the electronic bandstructure, which provide necessary information for transparent conductive behavior with electron doping. The presence of a broad CB, and a low carrier effective mass reflect the needs for substantial metal–metal contacts in the crystal structure.[5]

Although the carrier generation mechanism in bixbyite IZTO materials has been investigated broadly, there is never an agreement on the origin of free carriers. Investigations on the charge transport are scarce. The current challenge is to understand the relationship between their structure and their optoelectronic properties. It is still somewhat unclear how Sn/Zn defects or complexes would distribute and interact with each other in In_2O_3 lattice, and thus how can they affect the conductive performances, i.e., the free carrier generation and the charge transport mechanism. We realize that Zn plays the key role in IZTO materials. But compared with ITO, IGZO or In-Cd-Sn-O etc. systems, we do not have the detailed and systematic knowledge about the key role of Zn dopant in IZTO materials. Only when we obtain such understanding, could we control and design new materials with customized properties.[51] Thus we carry out a series of theoretical studies on the carrier generation and charge transport mechanism of IZTO. By analysing of the variation of the bandstructure caused by the composition change, we find that the existence of Zn ions could be helpful in controlling the electronic and optical properties of IZTO materials.

Modeling and Computation methods

As confirmed by experimental observations, the parent compound of IZTO solid solution is In_2O_3. In_2O_3 (JCPDS Card No. 6-416) crystallizes in the C-type rare-earth (bixbyite) structure (space group Ia3, number 206).[35] So we adopt the bixbyite structure to simulate In_2O_3 and IZTO systems with various defects, as shown in FIG.1 (a). The bixbyite structure can be derived from the fluorite structure with one quarter of anions missing, resulting in a periodic structure with structural vacancies, which are marked as green balls in FIG.1(b). In_2O_3 unit cell has 80 atoms, 32 of which are indium cations. All indium cations are surrounded by six oxygen atoms and

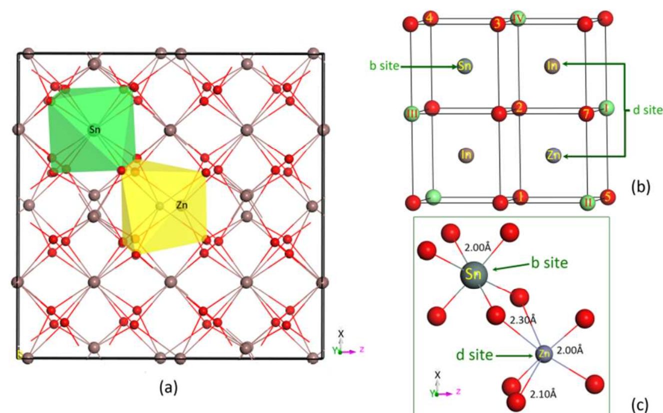

FIG.1. (a) Geometry structure of IZTO crystal. Lattice positions of Zn and Sn are marked accordingly with illustrations of corresponding SnO6 (green) and ZnO6 (yellow) octahedrons, respectively. The red and ocherous balls represent the oxygen and indium atoms, respectively. (b) The schematic plot of the cation-oxygen octahedrons around Zn/Sn pair in bixbyite structure, where Sn locates at b-site and Zn locates at d-site, respectively. The green balls represent the structural vacancies. The numbers 1~7 denote positions of VO defects and the numbers I~IV denote positions of Sni or Oi in various defective configurations. (c) The optimized local structure of ZnO6 and SnO6 octahedrons. The bond lengths are also given

Journal of Materials Chemistry C Accepted Manuscript

This journal is © The Royal Society of Chemistry 20xx

Please do not adjust margins

accordingly.

two structural vacancies, while all oxygen atoms are 4-fold coordinated. Indium cations locate at two crystallographically distinct sites: the b-site (8 atoms, 25%) and the d-site (24 atoms, 75%).[52] At b-site, two structural vacancies sit at body diagonal positions with equidistance In-O bond lengths of 2.18 Å. At d-site, two structural vacancies sit at face diagonal positions with pairs of In-O bond lengths of 2.13, 2.19, 2.23 Å, respectively.

First-principle calculations based on density functional theory implemented in *Vienna Ab initio Simulation Package (VASP)*[53, 54] have been carried out. The electron-electron exchange and correlation effects are described by generalized gradient approximation (GGA) functional with Perdew-Burke-Ernzerhof (PBE) method.[55] GGA+U method[56] is used to correct the band gap underestimtion of transition or post-tansition oxides. The on-site coulomb energy U are set to 7.5 eV, 7.0 eV, 7.0 eV for *d*-orbitals of Zn, In and Sn atoms, respectively.[57-59] The electronic wave functions are expanded using projector augmented wave method[60] with a cutoff kinetic energy of 400 eV. The geometry optimization procedure for the supercell is performed based on the minimization of total energies and forces, where the minimum energy state is achieved by relaxing the internal position of atoms and lattice parameters until the residual force is 0.01 eV/Å. The self-consistent convergence accuracy is set to 10^{-6} eV. A 3×3×3 Monkhorst-Pack mesh is used to integrate the first Brillouin zone.

Geometric structures and thermodynamics

Single dopant

As is well known, the physical property of TCOs is tuned by its chemical compositions, i.e., the spatial distributions of defects or defect associates. The geometric configurations of Sn/Zn cosubstitued In_2O_3 (IZTO) materials with intrinsic or extrinsic defects affect the electronic properties in different ways. The spatial distributions of defects, including the concentration and the location, can be represented by the formation energies, which are calculated by the formula given below

$$\mathrm{E}^{for} = E_{tot}^{\alpha} - E_{tot}^{perfect} + \sum_i n_i \mu_i \qquad (1)$$

Here E_{tot}^{α} and $E_{tot}^{perfect}$ are the total energies of the supercell with defect α and the perfect In_2O_3 supercell, respectively. n_i is the element i added to (n_i<0) or removed from (n_i>0) the perfect supercell to form a defective supercell. μ_i is the chemical potential of the element i (i = In, Zn, Sn and O). These chemical potentials are subjected to the thermodynamic boundary conditions that the chemical potential for the compound equals to the sum of chemical potentials of constitution elements, for instance, $\mu_{In2O3} = 2\mu_{In}+3\mu_O$, $\mu_{ZnO} = \mu_{Zn}+\mu_O$, and $\mu_{SnO2} = \mu_{Sn}+2\mu_O$. Therefore, chemical potentials of In, Sn, Zn and O are dependent on each other. In the calculation procedure for formation energy, we consider two limiting cases: the oxygen-rich limit and the indium-rich limit. In the oxygen-rich limit, μ_O equals to the value obtained from the oxygen molecule, while $\mu_{In}= (\mu_{In2O3}-3\mu_O)/2$. When the cases come to indium-rich, μ_{In} equals to the value obtained from the indium metal, while $\mu_O= (\mu_{In2O3}-2\mu_{In})/3$. It is possible for defects to agglomerate and form complexes. The spatial distribution of the defect associate in In_2O_3 lattice is not only represented by the formation energy, but also determined by the binding energy E^b, the energy gained in the reaction to form the complex by two or more isolated defects. This binding energy E^b between the constituent A and B can be defined in terms of their formation energies as below:[61]

Table 1. The formation energies and the lattice parameters of stoichiometric In_2O_3, single Sn doped In_2O_3 at position d- and b-site (denoted as ITO_d and ITO_b, respectively), and single Zn doped In_2O_3 at position d- and b-stie (denoted as IZO_d and IZO_b, respectively), the Zn/Sn codoped In_2O_3 (namely, IZTO), IZTO with Zn being fixed at the central site of ZnO_6 octahedron (denoted as IZTO_center), and IZTO configurations with intrinsic and correlated complexes, respectively.

Configurations	Lattice parameter (Å)	Formation energy (eV)	
		O-rich	In-rich
In_2O_3	9.95	--	--
ITO_d	9.94	2.37	0.45
ITO_b	9.93	2.22	0.30
IZO_d	9.92	1.41	3.32
IZO_b	9.92	1.49	3.39
IZTO	9.90	0.87	0.85
IZTO_center	9.90	1.03	1.01
In_2O_3:V_O	9.93	5.20	1.35
IZTO:Vo	9.89	5.67	1.80
IZTO:O_i	9.92	2.08	5.91
IZTO:Sn_i	9.99	13.80	6.09
IZTO:$2Zn_{In}$-V_O	9.90	4.16	2.19
IZTO:$2Sn_{In}$-O_i	9.91	3.31	5.21
IZTO:$2Sn_{In}$-Zn_{In}	9.90	2.87	0.92

$$E^b = \left(E^{for}(\mathrm{A}) + E^{for}(\mathrm{B})\right) - E^{for}(\mathrm{AB}) \qquad (2)$$

In this work, we only consider the defects/complexes related to the electronic properties in In_2O_3 lattice. The calculated data using equation (1) are listed in Table 1 and the corresponding interpretations are expressed below.

Firstly, we consider four single-cation substitution configurations in In_2O_3: Zn single substitution of In atom at nonequivalent b- or d-site (signaled as $Zn_{In\text{-}b}$ and $Zn_{In\text{-}d}$), respectively; Sn single substitution of In atom at nonequivalent b- or d-site (signaled as $Sn_{In\text{-}b}$, $Sn_{In\text{-}d}$), respectively. In particular, when In_2O_3 crystal is doped solely by Sn impurity, it is actually the commonly called ITO materials. The data listed in Table 1 show that Sn dopant prefers to occupy the b-site in In_2O_3, which is in accord with the experimental observations.[62] In this configuration, all six Sn-O bond lengths are almost equivalent in the value of 2.01Å, and the local symmetry of Sn-O octahedron resembles the case in bulk SnO_2 materials. In contrast, when Zn species are doped into In_2O_3 systems, they favor to substitute the d-site, i.e., the lower symmetry site, in which configuration six Zn-O bond lengths are 2.01/2.14/2.18 Å, respectively.

Journal of Materials Chemistry C Accepted Manuscript

Please do not adjust margins

Zn and Sn cosubstitution

Secondly, we investigate the formation of IZTO supercell, i.e., Zn/Sn impurity pairs being codoped into In_2O_3 supercell. As the codoping is a complicated behavior, six configurations are explored. In the first step, we adopt two Sn/Zn codoping configurations: (1) Zn locating at b-site and Sn locating at d-site; (2) Zn locating at d-site and Sn locating at b-site. Then in each of these two Sn/Zn configurations, the separation between Sn and Zn are arranged to be near, medium and far. After relaxations for these six configurations, the configuration containing Zn/Sn impurity arranged in the nearest neighboring to each other has the lowest formation energy. In other words, Zn and Sn dopant prefer to occupy the nearest neighboring edge-sharing metal-oxygen octahedrons. If the separation between Zn/Sn pairs keeps instant, the configuration with Zn at d-site and Sn at b-site has a lower energy than the other configuration, which is already implied by conclusions from the isolated Zn- or Sn-doped In_2O_3 systems. That is to say, for stoichiometry conditions, the configuration containing Zn at d-site and Sn at b-site with the nearest separations between them has the lowest system energy. So we refer to this kind of configuration as IZTO system in the following discussions, unless we make specific notation. As listed in Table 1, the formation energies of IZTO under O-rich and In-rich limitations are 0.87 eV and 0.85 eV, respectively. The binding energy of this Sn_{In}-Zn_{In} complex equals to 2.77 eV. It is a common knowledge that only having a positive binding energy does not mean a complex will necessarily form. The constituents and complexes are governed by thermal equilibrium at the growth temperature. To obtain the higher concentration of complexes than that of either constituent, its formation energy should be lower than both E^{for} of isolated defects.[61] This immediately implies that the binding energy E^b needs to be larger than either of $E^{for}(A)$ and $E^{for}(B)$. In other words, unless the binding energy of the complex is larger than the formation energy of the constituents, its concentration will be small. Therefore, it is evident that Zn_{In}-Sn_{In} complex should be codoped into In_2O_3 supercell easier than isolated Sn_{In} or Zn_{In} defect during IZTO materials preparation process.

The enhancement of Zn/Sn pairs codoping in In_2O_3 lattice is consistent with the experimental observations that codoping could increase the solubility greatly,[34, 35] which is ascribed to the isovalent substitution of two In^{3+} ions with a Sn^{4+} and a Zn^{2+} ions. For ITO materials, when the isolated Sn_{In} defect forms, for the reason of Sn^{4+} is a tetravalent ion with respect to In^{3+} ion, it would induce an extra free electron. As reported previously, wavefunctions of extra free electron are so dispersed that it could produce a local repulsive stress in the lattice,[63, 64] and thus the variation of electronic environment limits the solubility of Sn_{In} defect. The electronic environment effect is also confirmed by the change of lattice parameters during the substitution process. The radii of Sn^{4+}, Zn^{2+} and In^{3+} are 0.69Å, 0.74Å and 0.80Å, respectively, so the Zn^{2+} and Sn^{4+} substitution decrease lattice parameters of In_2O_3. In general, the decrease arising from Sn^{4+} doping should be larger than that induced by Zn^{2+} doping, as a result of the smaller radius of Sn^{4+} than Zn^{2+} ion. However, the data listed in Table 1 show that the reverse is the truth. The decrease of the lattice parameter induced by Sn_{In} is smaller than that induced by Zn_{In} defect, because Sn_{In} defect induces extra free electrons and thus generates the local electronic compression in the lattice, which makes lattice expand and hinders the lattice parameter decrease effect yielded by the radius difference between Sn^{4+} and In^{3+} ions. Nevertheless, when In_2O_3 system is cosubstituted by Zn^{2+}/Sn^{4+} pair of two In^{3+} ions, the hole created by Zn_{In} defect could combine with the extra electron induced by Sn_{In} defect. The charge neutralization weakens the lattice distortion caused by the electronic environment variation and so increases the solubility of Zn and Sn dopant both. This agrees well with previous reports that codoping with two acceptors with a donor or an isovalent impurity could lead to a favoured impurity complex. By choosing the codoping elements carefully, the complex could increase the solubility of the desired dopants.[65-67] As a result, the unit cell gets smaller with the cosubstitution of Zn/Sn dopant, following Vegard's rule, as confirmed by the X-ray reflection measurements.[34, 35]

In IZTO, Zn and Sn locate at d- and b-site, repetively, and occupy two edge-sharing octahedrons to form the nearest Sn/Zn cation pairs, where two oxygen aotms are shared. Optimized SnO_6 and ZnO_6 octahedrons are shown in FIG.1(c). The SnO_6 octahedron reserves the local symmetric environment as the b-site InO_6 octahedron in undoped In_2O_3, where Sn atom locates at the center of SnO_6 octahedron, and the six Sn-O bond lengths are all about 2.00Å, with slightly variation not larger than 0.04Å. However, the symmetric environment around ZnO_6 octahedron gets worse than undoped d-site InO_6 octahedron. Zn atom displaces manifestly from the center of ZnO_6 octahedron, with the six Zn-O bond lengths in values of 2.00/2.10/2.30 Å, respectively. It is ascribed to the reason that the local structure of Zn atom under normal conditions is ZnO_4 tetrahedron. The obvious difference between the local structure in

This journal is © The Royal Society of Chemistry 20xx

Journal of Materials Chemistry C Accepted Manuscript

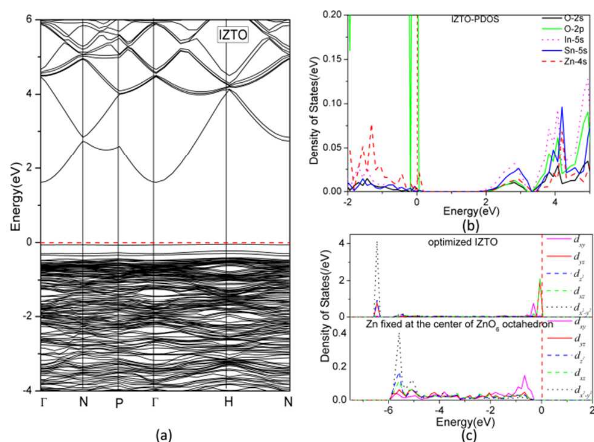

FIG. 2. (a) The bandstructure of IZTO. (b) PDOS of constituent elements in IZTO. (c) PDOS of Zn-3*d* orbitals distributed near VBM in relaxed IZTO supercell and in unrelaxed IZTO supercell with Zn atom being fixed at the center of ZnO_6 octahedron, respectively. In these three plots, the red dashed lines represent Fermi level.

ZnO_4 and ZnO_6 polyhedrons makes Jahn-Teller effect occur to worsen the geometric symmetry around Zn and adopt a lower energy state, just as verified in ZnO and other materials.[68-70] To verify this imagination, we construct an IZTO configuration with Zn atom fixed at the center of ZnO_6 octahedron, i.e., a better symmetric atomic arrangement. As listed in Table 1, the calculated system energy of this configuration is really larger of 0.16 eV than the one with worse symmetric configuration. The plot in FIG.2(c) show that Jahn-Teller effect can also be clearly confirmed by projected density of states (PDOS) of Zn, where the nondegenrate Zn-3*d* orbitals are illustrated by the sharp separated peak, originating from the crystal field splitting.

In particular, the two Zn-O bonds in length of 2.30 Å are formed by Zn atom with the two oxygen atoms being shared by ZnO_6 and SnO_6 octahedrons. They are too long to form strong Zn-O bonds in comparison with the rest four Zn-O bonds, or we can say that these two oxygen atoms move towards Sn site. This kind of geometric structure makes the coordination numbers of Sn and Zn atoms in IZTO change and become nonequivalent. In experimental measurements the coordination number around Zn is found to be less than 6 (the normal number in InO_6 octahedron),[71] while the coordination number around Sn is estimated to be larger than 6, which are called undercoordination of Zn and overcoordination of Sn, respectively. This phenomenon can be explained quite well by our analyses about the SnO_6 and ZnO_6 octahedrons. It is proposed that the undercoordination of Zn and overcoordination of Sn are generated by the oxygen transition from ZnO_6 octahedron to SnO_6 octahedron. Therefore, we investigate two oxygen transition paths from ZnO_6 octahedron to SnO_6 octahedron. In path 1, oxygen atom moves from position 7 to position III, and in path 2, oxygen atom migrates from position 1 to position IV, where the numbered positions are marked in FIG.1(b). Finally, we find that transition barriers of both paths are so large that the oxygen transition will not possible take place actually.

Intrinsic defects

The intrinsic defects V_O, O_i and Sn_i in IZTO and their complicated complexes including $2Zn_{In}$-V_O, $2Sn_{In}$-O_i and $2Sn_{In}$-Zn_{In} defects that may be related to the n-type conduction are also investigated consequently. According to previous studies reviewed in the introduction section, V_O and O_i are the most favorable intrinsic defects that influence the n-type carrier generation. For V_O defect in IZTO, we examine six different V_O arrangements to estimate the influence brought by defect positions to the formation energies. In five of these six configurations, V_O positions are marked as number 1~5 in FIG.1(b), respectively, which all lie in ZnO_6 or SnO_6 octahedrons. Meanwhile, we construct the sixth configuration with a V_O defect at site 6 (not shown here) far away from ZnO_6 or SnO_6 octahedrons. We find that the position of V_O really affect the formation energy. The most favorable position for V_O in IZTO lattice is the site 1 in ZnO_6 octahedron, the most unfavorable positions are site 3 and 4 that surrounding the SnO_6 octahedron, the formation energy of V_O locating at the site 6 (in InO_6 octahedron) lies in the medium range. When the case turns to be O_i in IZTO, we also construct four configurations in which O_i defects locate at the four structural vacancies in ZnO_6 and SnO_6 octahedrons, and these positions are denoted as number I~IV in FIG. 1(b). We just consider the structural vacancy positions because it has been already proved that within the bixbyite lattice, the structural vacancy sites are the most favorable sites for interstitial defects.[72] Calculations of formation energy for these four O_i containing IZTO configurations show that O_i also prefers to occupy the site I, i.e., the position within ZnO_6 octahedron, not lies in SnO_6 octahedron. So we come to the conclusion that no matter IZTO system trap excess oxygen atoms or lose oxygen atoms from stoichiometric chemical composition, the reaction process always prefers to take place in ZnO_6 octahedron.

This conclusion derives from the fact that compared with Sn-O bonds, Zn-O bonds are easier to break to form the corresponding defect. This result is in accord with the experimental observations that oxygen content mainly influences Zn atoms, not Sn atoms in In_2O_3-based materials.[33, 73] This phenomenon can be interpreted by two reasons. The first reason is that normally, Zn atom is 4-fold coordinated, while in IZTO system it is 6-fold coordinated, hence the lattice distortion induced by Zn in this system is so large to make Zn-O bond being broken easily. However, Sn atom in IZTO system lies at b-site, where six Sn-O bonds almost have the equivalent bond lengths. The local structure in this kind of SnO_6 octahedron is more symmetric, so breaking this kind of Sn-O bond requires more energy in the formation of V_O or O_i defect. The second reason is that the energetics of different site locations of the oxygen defect in multicomponent TCOs correlates with the formation energy of the constituting single-cation oxides,[12] which are -7.69 eV/O_2, -8.39 eV/O_2 and -10.51 eV/O_2 for In_2O_3, ZnO and SnO_2, respectively. The most preferred location of the oxygen

Journal of Materials Chemistry C Accepted Manuscript

This journal is © The Royal Society of Chemistry 20xx

Please do not adjust margins

vacancy or interstitial corresponds to the selection of the metal-oxygen bonds that would be easiest to break during the creation of defects, namely, the site in ZnO_6 octahedron with three In and one Zn neighbors. Comparing the two intrinsic oxygen defect in IZTO system, i.e., V_O and O_i, although the formation energy of O_i is smaller than that of V_O under O-rich condition, the average formation energy of which is slight larger than that of V_O defect. This results from that when O_i is pushed into IZTO lattice, it produces local compressive force to make lattice expand, which is energy consumable. So based on discussions above, although the formation energy of V_O in IZTO system is slightly larger than that of V_O in In_2O_3 system, the existence of Zn atoms in IZTO lattice may benefit the formation of V_O, that is, be helpful to generate n-type carriers.

Complexes

There are some investigations suggesting that the cosubstituted sample has a slight imbalance of Sn^{4+} compared to Zn^{2+}, and the excess Sn^{4+} would then acts as net donor.[35, 37] It is also proposed that $2Sn_{In}$•O_i complex would be partially responsible for the observed conductivity variation under different preparation or treatment conditions. Therefore, we study the Sn-excess crystalline by inserting Sn_i, Sn_{In} and Sn_{In}-O_i into IZTO lattice to form Sn_{In}-Zn_{In}-Sn_i, $2Sn_{In}$-Zn_{In} and $2Sn_{In}$-O_i complexes, respectively. Six configurations are constructed to simulate Sn_{In}-Zn_{In}-Sn_i complex system. Four of them are constructed with Sn_i defect locating at structural vacancies within ZnO_6 and SnO_6 octahedrons, which are numbered as I~IV in FIG. 1(b). In other two configurations, Sn_i locating at sites far away from ZnO_6/SnO_6 octahedrons (not shown here). For $2Sn_{In}$-O_i and $2Sn_{In}$-Zn_{In} complexes system, we construct three configurations for each of them, respectively. In each case, the separation between the second Sn_{In} and Sn_{In}-Zn_{In}/O_i cluster varies from near to far. Calculated results show that the formation energy of systems containing interstitial defect is large, for instance, Sn_i defect in IZTO has the formation energy larger than 6 eV, implying it is difficult to form in the prepare process. The smallest formation energy of 0.92 eV is attributed to one of $2Sn_{In}$-Zn_{In} configurations, in which the second Sn_{In} defect also locates at b-site and is far away from the original Zn_{In}-Sn_{In} cluster. The binding energy of $2Sn_{In}$-Zn_{In} complex is 3.00 eV, that is, this complex is thermodynamic stable in IZTO materials. We also examine another defect associate $2Zn_{In}$•V_O complex that is suggested to account for the conductivity change affected by the atmosphere condition. As listed in Table 1, this complex possesses moderate formation energy and may have an unneglected influence on the conductive behaviour of IZTO.

It is evident from analyses mentioned above that Zn/Sn cluster can be easily cosubstituted into In_2O_3 lattice as a result of the very low formation energy, meaning the bixybite IZTO can be obtained easily. The n-type carriers in IZTO may be predominantly contributed and affected by defects or associates including V_O and Sn_{In}. The existence of Zn_{In} defect is beneficial to form V_O or Sn_{In} related defects. Nevertheless, we should note that the n-type conductivity of IZTO cannot be determined only by the carrier generation mechanism, but also determined by the charge transport mechanism, i.e., carrier mobility or effective mass. In general, the charge transport mechanism can be illustrated by details of electronic structures, so we present the corresponding analyses about the electronic structures of IZTO in the next section.

Bandstructure and Charge transport

Stoichiometric and isolated Sn or Zn doped In_2O_3

Firstly, the bandstructure of undoped bixbyite In_2O_3 crystal is calculated and shows the indirect band gap in value of 1.92 eV. As plotted in FIG.3(a), the energy difference between the direct and indirect band gap is less than 35 meV, according with previous reports.[12, 51, 57, 62, 74] The detailed electronic structures are demonstrated by the total density of states (DOS) and atomic projected density of states (PDOS), as shown in FIG.3(b). The energy dispersion of the conduction band arising from In-5*s*/O-2*p* overlap determines the charge transport properties in semiconductor materials. It is already proposed that the lowest effective mass chemistries are correlated with a strong *s*-orbital character in CBM,[6] while compounds with large *d*-orbital character at CBM have much

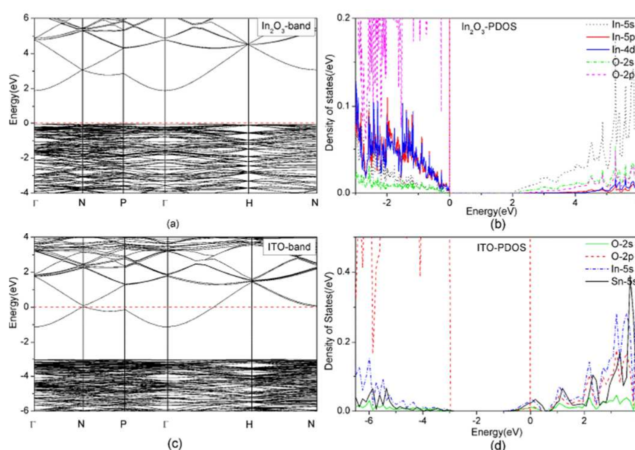

FIG.3. (a) The bandstructure and (b) PDOS of In_2O_3, respectively. (c) The bandstructure and (d) PDOS of ITO crystals, respectively. The red dashed lines in these plots represent Fermi level.

larger electronic effective mass. In addition to a *s*-orbital character, the cation orbitals need to hybridize adequately with oxygen orbitals. DOS of bixbyite In_2O_3 show that the bonding and nonbonding O-2*p* states form the valence band (VB), while CB is comprised of the antibonding state yielded by the strong In-5*s*/O-2*p* interactions. The empty In-5*p* states form the following band at a higher energy. PDOS plotted in FIG. 3(b) reveals that O-2*p* and In-5*s* states make comparable contributions to the bottom of CB. The precise contributions are listed in Table 2, where we integrate the corresponding curve area arranged over the bottom of CB to represent the orbital-dependent contributions from constituent atoms in the lattice. For all systems, we calculate the average contributions from all of the oxygen and indium species and denote

This journal is © The Royal Society of Chemistry 20xx

Journal of Materials Chemistry C Accepted Manuscript

them as O(A) and In(A) in Table 2. Contributions to CB derived from the isolated oxygen or indium atoms in this lattice are also calculated. Calculated data tells us clearly that contributions supplied by isolated In and O atom are nearly similar, and more than 80% and 50% of each contribution come from In-5*s* and O-2*p* orbitals, respectively. DOS projected on In atom at b-site and d-site exhibit nearly same characteristics, meaning the nonequivalent geometric positions of cation show little influence on the electronic contributions of In species. Therefore, the bottom of CB originates primarily from the hybridization between the *s*-orbital of cation and the antibonding *p*-orbital of oxygen atoms. Clearly, the *sp* hybridization provides the uniform charge distribution within the In_2O_3 cell, which constructs a three dimensional In-5*s*/O-2*p* network for charge transport once extra carriers fill the band.

As discussed above, when an isolated Sn atom substitute the b-site In atom in In_2O_3 lattice, namely, forming ITO materials, the band gap turns to be 1.88 eV, which is slightly less than the band gap of the original In_2O_3 material. The impurity states induced by Sn_{In} defect hybridize strongly with the bottom of CB, turning this material to an n-type degenerate semiconductor. Fermi level is pinned into CB and lies at the position of 1.13 eV above CBM.

Table 2. Contributions to the bottom of conduction band projected on constituent elements in IZTO and other In_2O_3-based TCOs. In the first row, the average contributions from all of the oxygen atoms and all of the indium atoms in lattice are denoted as O(A) and In(A), respectively. O(1), O(2), O(3), In(1) and In(2) denote contributions from oxygen and indium atoms, where the distance between them and the induced defects increases from near to far, respectively. The phrase "total" in the second column represents the total contributions summed over a specific atom. The characters *s*, *p*, *d* in the second column represent the corresponding atomic orbital contribution ratio of total contributions. The total value O(A) is set as a standard value (denoted as 1.00), and total contributions from other atoms are expressed as the ratio of the standard value (the total value O(A)). All values are in units of eV.

Configurations	Orbitals	O(A)	O(1)	O(2)	O(3)	In(A)	In(1)	In(2)	Sn	Zn
In_2O_3	*s*	46.67%	46.67%	--	--	84.00%	84.00%	--	--	--
	p	53.33%	53.33%	--	--	8.00%	8.00%	--	--	--
	d	--	--	--	--	8.00%	8.00%	--	--	--
	Total	1.00	1.00	--	--	1.67	1.67	--	--	--
ITO	*s*	50.00%	53.85%	46.15%	--	83.33%	80.95%	83.33%	82.61%	--
	p	50.00%	46.15%	53.85%	--	8.33%	9.52%	8.33%	8.70%	--
	d	--	--	--	--	8.33%	9.52%	8.33%	8.70%	--
	Total	1.00	0.93	0.93	--	1.71	1.50	1.71	1.64	--
In_2O_3:Zn	*s*	46.15%	41.67%	50.00%	--	83.33%	80.95%	81.48%	--	83.33%
	p	53.84%	58.33%	50.00%	--	8.33%	9.52%	7.40%	--	8.33%
	d	--	--	--	--	8.33%	9.52%	11.11%	--	8.33%
	Total	1	0.93	1.08	--	1.85	1.62	2.08	--	0.93
IZTO	*s*	50.00%	41.67%	53.85%	46.15%	83.33%	80.95%	81.82%	80.00%	75.00%
	p	50.00%	58.33%	46.15%	53.85%	8.33%	9.52%	9.09%	10.00%	16.67%
	d	--	--	--	--	8.33%	9.52%	9.09%	10.00%	8.33%
	Total	1.00	0.86	0.93	0.93	1.71	1.50	1.57	1.43	0.86
$In_2O_3:V_O$	*s*	42.86%	14.29%	41.67%	50.00%	65.39%	23.38%	76.00%	--	--
	p	57.14%	85.71%	58.33%	50.00%	19.23%	49.35%	12.00%	--	--
	d	--	--	--	--	15.39%	27.27%	12.00%	--	--
	Total	1.00	1.50	0.86	0.86	1.86	5.50	1.79	--	--
IZTO:V_O	*s*	40.00%	15.79%	38.46%	50.00%	67.86%	28.33%	79.17%	70.00%	45.45%
	p	60.00%	84.21%	61.54%	50.00%	17.86%	43.33%	8.33%	15.00%	27.27%
	d	--	--	--	--	14.29%	28.33%	12.50%	15.00%	27.27%
	Total	1.00	1.27	0.87	0.93	1.87	4.00	1.60	1.33	0.73
IZTO:$2Sn_{In}$-Zn_{In}	*s*	50.00%	42.86%	50.00%	53.33%	83.33%	80.65%	80.65%	81.81%	76.92%
	p	50.00%	57.14%	50.00%	46.67%	8.33%	9.68%	9.52%	9.09%	15.39%
	d	--	--	--	--	8.33%	9.68%	9.52%	9.09%	7.69%
	Total	1.00	1.00	1.00	1.07	1.71	2.21	1.50	1.57	0.93

Beyond this, the bandstructure of ITO changes little compared with that of In_2O_3, which agrees well with previous investigations.[12] As demonstrated in FIG.3(c) and (d), TDOS and PDOS of ITO show that contributions to the bottom of CB provided by In and Sn species are nearly identical, and more than 80% of their contributions are attributed to In-5*s*/Sn-5*s* orbitals. No matter the indium atom locates at b- or d-site, its contribution keeps nearly constant. O-2*p* orbitals provide similar contributions as it does in In_2O_3 lattice. This means that the strong hybridization between In/Sn-5*s* and O-2*p* orbitals gives birth to a nice charge transport path to make the free carriers distribute over the lattice uniformly. Therefore, free carriers generated by Sn_{In} defects can transport in the conduction band effectively, leading to a very nice conductivity of ITO materials.

When Zn is single doped into In_2O_3 lattice and occupy the d-site, as there is one less valence electron for Zn^{2+} than In^{3+} ion, Fermi

Journal of Materials Chemistry C Accepted Manuscript

This journal is © The Royal Society of Chemistry 20xx

Please do not adjust margins

level is pinned into valence band and makes this system show p-type conductivity. Except this, the near edge band structure changes little, which is plotted in Fig. S1 (a) in supplementary materials, similar as the case in Sn-doped In_2O_3. However, if extra electrons produced by intrinsic or extrinsic defects emerge and compensate the holes induced by Zn_{In} defects (actually, it is easy to happen), the transport properties near CBM are also important characters to explore. The hybridization near bottom of CB is made up with In-5*s*/Zn-4*s* orbitals, as shown in Fig.S1 (b). Detailed contributions from constituent elements electronic orbitals to CBM are also calculated and listed in Table 2. The contribution distributions nearly resemble that of the Sn doped In_2O_3, but contributions from the Zn dopant atomic orbitals is less than that of In and Sn ions, which is caused by the large lattice distortion discussed above and is disadvantaged for charge transport.

IZTO materials

When IZTO crystals is formed, i.e., Zn and Sn atoms are codoped of d-site and b-site In atoms in In_2O3 lattice, respectively, minor changes of the bandstructure occurs in comparison with that of In_2O_3 and ITO materials. For the neutralization of Zn^{2+} and Sn^{4+}, the highest occupied electronic state shifts downward to the valence band maximum (VBM). It also has an indirect band gap with energy difference between direct/indirect band gaps of 0.02 eV. The fundamental band gap is 1.66 eV, and this value is slightly less than the original In_2O_3 materials, which agrees well with the experimental observations.[35, 43] As similar as cases of IGZO [12, 13] and $Cd_{1+x}In_{2-2x}Sn_xO_4$ systems,[17] Palmer et al. found that heavy cosubstituted IZTO sample had a slightly narrower band gap than the less cosubstituted sample and proposed that this band gap narrowing is ascribed to the donor-acceptor pairs formed with Zn^{2+} and Sn^{4+}.[35] The band gap narrowing phenomenon, or we call it the *band gap renormalization effect*, results from the electron-electron and electron-ionized impurity interactions.[75] This effect can also be verified from analyses of DOS in FIG.2 (b) and (c) for IZTO systems. As discussed in Section III.B, the large lattice distortion of ZnO_6 octahedron due to Jahn-Teller effect makes the crystal field around Zn splits, resulting in the nondegeneration of Zn-3*d* orbitals. The nondegenerate Zn-3*d* orbital is demonstrated by the sharp and strong peak in the top of VB, which resonants strongly with the nearest Sn-5*d*/In-5*d*/O-2*p* orbitals and thus shifts VBM upward to narrow the band gap.

The wavefunctions of conduction band in IZTO are also analyzed to investigate the transport properties tuned by the cosubstitution of Zn^{2+}/Sn^{4+} in In_2O_3. In accord with the hybrid nature of the bottom of the CB, all atoms in IZTO unit cell give comparable contributions to the conduction band wavefunctions. If the average contributions from all of the oxygen atoms (denoted as O(A) in Table 2) in the supercell is set to be unit, contributions from oxygen with different distances away from Zn^{2+}/Sn^{4+} pair equal to nearly identical value, just as the case in In_2O_3 and ITO materials. All cations, i.e., Zn, Sn and In, contribute considerable to the bottom of CB. Both In-5*s* and Sn-5*s* provide comparable contributions in value of about 1.50 times of O(A). Nevertheless, both *s*-orbitals of In and Sn contribute more than 80% of their total contributions, which make free

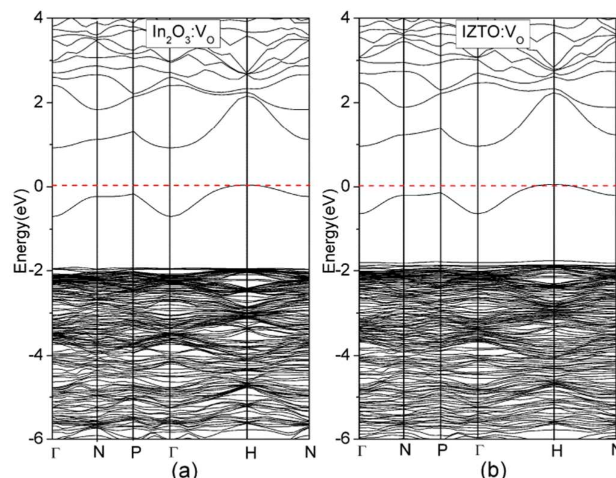

FIG. 4. Bandstructures of (a) In_2O_3:V_O and (b) IZTO:V_O materials, respectively. The red dashed lines in these two figures represent Fermi level.

carriers transport in IZTO lattice in a large velocity and thus can distribute uniformly. However, the contribution to CBM yielded by Zn atom is about 0.50 times of the value induced by Sn/In species, and the *s*-orbital contribution ratio of total is 75.00%. Meanwhile, contribution from *p*-orbitals increases to 16.67%. This is also a result of the large lattice distortion around ZnO_6 octahedron after geometry optimization. As discussed in section III.B, the worse symmetry weakens the interaction between Zn and two O atoms, while drives Zn to bond more strongly with other four O atoms. That is to say, Zn tends to recover to the ZnO_4 tetrahedron, just like in wurtzite ZnO crystal. This change makes the Zn-O bond show more covalent characters and strengthens Zn-*p*/O-*p* bonding interaction, which is directionality and thus decrease the ability to transport free carriers.

Different localization induced by V_O defect in In_2O_3 and IZTO materials

It is well know that oxides composed of post-transtition metals favor large oxygen deficiencies even under equilibrium conditions. Removal of an oxygen atom from oxides leaves two extra electrons in the crystal and the observed conductivity in oxides is attributed to the exited oxygen vacancy, i.e., V_O^{1+}etc.[12] Therefore, oxygen vacancies put important impaction on the conductivity of metal oxides. The bottom structure of CB could be affected by oxygen vacancies manifestly and give rise to different transport and optical properties. Hence we plot bandstructures of In_2O_3:V_O and IZTO:V_O systems in FIG.4 and make a corresponding comparison between their conductive difference. It is clearly illustrated in the bandstructure of In_2O_3:V_O system in FIG.4(a) that there is a fully occupied impurity states lying in the band gap, which is

Journal of Materials Chemistry C Accepted Manuscript

This journal is © The Royal Society of Chemistry 20xx

nonconductive. Compared with stoichiometric In_2O_3, addition of V_O defect changes the constituent elements generating contributions to the bottom of CB obviously, as listed in Table 2. There are two main changes emerge: (1) Contributions from the nearest neighboring (NN) In and next nearest neighboring (NNN) O atoms increase manifestly, and are in values of 1.50 and 5.50 times of the standard value O(A), respectively. (2) Contributions from *p*/*d* orbitals are strengthened, for example, 2*p* orbital of NNN O(1) atom contributes 85.71% of total, which is larger than the value of original 53.33% in stoichiometric In_2O_3. At the same time, the contribution ratio of total from NN In(1)-5*p*/4*d* orbitals become 49.35%/27.27%, increase to 6 and 3 times of the original contributions in In_2O_3, respectively. The wavefunctions of *p*/*d* orbitals show evident directionality, which make the bond direction between cation and anion atoms, i.e., the charge transport path, anisotropic. Therefore, the localization effects appearing in both lattice space and atomic orbital decrease the charge transport ability of In_2O_3:V_O material.

When the material change to be IZTO:V_O, contributions to the bottom of CB supplied by constituent elements behaves just as in the case of In_2O_3:V_O systems: (1) Space localization. The NN In and NNN O species contribute most to the bottom of CB. (2) Orbital localization. Contributions from *p*/*d* orbitals to bottom of CB are large. But compared with In_2O_3:V_O system, these two localization effects are both weakened. For example, contributions from NN In and NNN O change to be 1.27 and 4.00 times of the standard value O(A), which decrease in an obvious manner. For NN In atom, the contribution ratio of total provided by its *s*-orbital increases evidently. These changes indicate that free carriers could transport through IZTO:V_O lattice easier than in In_2O_3:V_O lattice. This is also caused by the existence of Zn^{2+} in IZTO:V_O systems. From the calculated results given in Section III.C, V_O defect prefers to form in ZnO_6 octahedron instead of SnO_6 octahedron. When ZnO_6 octahedron lose an oxygen atom, the nominal coordination number of Zn decreases to five. One of the five remaining Zn-O bond lengths changes to be 2.26Å, which is longer than other four Zn-O bonds. In other words, the geometric environment around Zn is more like a tetrahedron. This local structure releases the lattice distortion around ZnO_5 polyhedron induced by V_O defect, thus it also weakens the disturbance on NN-In and NNN-O orbital wavefunctions generated by the lattice distortion of V_O. Nevertheless, the more closed tetrahedron around Zn makes the hybridization between Zn and O atoms become strong and the contributions supplied by *p*/*d* orbitals are promoted, as listed in Table 2.

Because of the localized mid gap states introduced by the oxygen vacancy, the transition energy barrier of the photon excitation from VBM and CBM can be reduced, which in turn will make the light absorption spectrum redshifts. But as discussed above, electronic orbitals of constituents interact with each other in complicated process and result in the upward shift of CBM, so the transparency of IZTO in solar spectrum is speculated to reserve in high value. However, this needs more proofs in experimental measurements in future work.

Bandstructure of $2Sn_{In}$-Zn_{In} cluster

The calculated formation energy results show that $2Sn_{In}$-Zn_{In} cluster has moderate formation energy and so has a certain chance to form. The bandstructure of IZTO system with $2Sn_{In}$-Zn_{In} cluster is similar as that of ITO. The impurity states generated by the extra Sn_{In} defect overlap with CBM, making this system to be a degenerate n-type semiconductor. Fermi level is pinned through CB at the energy level of 1.12 eV above CBM. The fundamental band gap is 1.84 eV, namely, nearly the same value of In_2O_3 and ITO. However, this band gap is 0.2 eV larger than that of IZTO, making it clear that the band gap narrowing is predominantly induced by Zn atoms in IZTO crystal. Contributions to the bottom of CB derived from constituent elements show similar characters with the situation in IZTO crystal, except that contributions from Sn and Zn increase slightly, and the contribution ratios of total from their *s*-orbitals are also promoted with a little value.

Conclusions

The main purpose of this work is making clear that in the new synthesized multicomponent IZTO materials, namely, Sn/Zn cosubstituted In_2O_3, how can these cosubsituted dopants interact with each other and how can they affect the electronic properties. From series of Density Functional Theory calculations, we can draw several important conclusions:

(1) In the formation process of stoichiometric IZTO, the calculated formation energy and the binding energy show that the solubility of codoped Zn/Sn dopants are both promoted greatly than isolated Sn_{In} or Zn_{In} defect in In_2O_3. This is attributed to the isovalent substitution of a Sn^{4+}/Zn^{2+} pair for two In^{3+} ions. The emergence of Zn^{2+} releases the lattice distortion originating from isolated ${Sn_{In}}^{4+}$ defect.

(2) In thermodynamic stable bixbyite IZTO lattice, Zn and Sn atoms prefer to locate at the d-site and the b-site positions, respectively, and they tend to occupy the nearest neighboring octahedron to form Zn/Sn cluster. SnO_6 octahedron reserves the high local symmetry, while Jahn-Teller effect appears to worsen the geometric symmetry of ZnO_6 octahedron and adopt a lower energy configuration.

(3) There are two oxygen atoms shared by ZnO_6 and SnO_6 octahedrons. After optimization, these two oxygen atoms move closer to Sn atom, resulting in the undercoordination of Zn and overcoordination of Sn, respectively.

(4) Among intrinsic defects and complexes in IZTO, both V_O and O_i prefer to form in ZnO_6 octahedron, not in SnO_6 octahedron, because Zn-O bond is easier to break. The n-type carriers in IZTO may be predominantly povided by V_O and Sn_{In} defects and the correlated complexes for their relative lower formation energies. The existence of Zn_{In} is beneficial to form V_O or Sn_{In} related defects.

(5) Compared with In_2O_3 and ITO materials, the band gap renormalization effect narrows the band gap of IZTO. The crystal field splitting results in the nondegeneration of Zn-3*d* orbitals and thus shifts VBM upward to reduce the band gap. The role of Zn species on the band gap normalization is confirmed further in case of $2Sn_{In}$-Zn_{In} complex, where the additional Sn_{In} defect widens the band gap.

(6) An adequate hybridization between oxygen atoms and

Journal of Materials Chemistry C Accepted Manuscript

This journal is © The Royal Society of Chemistry 20xx

Please do not adjust margins

cations make all of these constituent elements, i.e., O, Zn, Sn and In, contribute comparable to the bottom of CB for In_2O_3-based TCOs. These contributions predominantly come from *s*-orbitals of cations and *p*-orbitals of oxygen atoms, which construct a three dimensional cation-*s*/O-2*p* network for charge transport. Both In-5*s* and Sn-5*s* in IZTO provide same contributions to the bottom of CB. However, the contribution from Zn atom is about half of the contributions from Sn/In species, and the *s*-orbital contribution of Zn decreases while the *p*-orbital contribution increases, resulting from the strengthening of the more covalent Zn-*p*/O-*p* interaction.

(7) When V_O is introduced into In_2O_3 or IZTO crystals, spatial localization and orbital localization in the conduction band emerge in both crystal, but the localization effect is weakened in IZTO crystals. The local structure around ZnO_5 polyhedron releases the lattice distortion induced by V_O defect, which weakens the disturbance on NN In and NNN O orbital wavefunctions and promotes the charge transport ability of IZTO:V_O compared with In_2O_3:V_O system.

Over all, the conductive properties of IZTO including the carrier generation mechanism and the charge transport ability can be tuned effectively by its chemical composition. The existence of Zn dopant increases the solubility of Zn/Sn pair and attracts V_O defect to generate free electrons. It induces bandstructure renormalization effect and strengthens the charge transport ability. Our works put forward the understanding on the micro mechanism of multicomponent TCOs materials and identify IZTO as an excellent candidate for the low indium content TCOs. Though these conclusions are obtained from analyses of In-Zn-Sn oxides, we believe they are also helpful in understanding other multicomponent TCOs materials.

Acknowledgements

This work is supported by the National Science foundation of China under Grant U1231103 and 41473065, and the Science Foundation for Youth of Shandong University at Weihai. The computations were carried out on a HP Proliant DL785G6 server hosted by the Institute of Space Sciences of Shandong University. We also thank Mrs Hongxia Zhang for the revision of English language in the preparation of this manuscript.

Notes and references

1 S. Lany and A. Zunger, *Phys. Rev. Lett.* , 2007, 98, 045501.
2 S. W. Heo, Y. D. Ko, Y. S. Kim and D. K. Moon, *Journal of Materials Chemistry C*, 2013, 1, 7009-7019.
3 D. E. Proffit, S. P. Harvey, A. Klein, R. Schafranek, J. D. Emery, D. B. Buchholz, R. P. H. Chang, M. J. Bedzyk and T. O. Mason, *Thin Solid Films* 2012, 520, 5633-5639.
4 F. Bonaccorso, L. Colombo, G. Yu, M. Stoller, V. Tozzini, A. C. Ferrari, R. S. Ruoff and V. Pellegrini, *Science*, 2015, 347, 1246501.
5 P. P. Edwards, A. Porch, M. O. Jones, D. V. Morgan and R. M. Perks, *Dalton Trans.* , 2004, 19, 2995-3002.
6 G. Hautier, A. Miglio, D. Waroquiers, G.-M. Rignanese and X. Gonze, *Chem. Mater.* , 2014, 26, 5447-5458.
7 M. Orita, H. Ohta, M. Hirano, S. Narushima and H. Hosono, *Philosophical Magazine Part B*, 2001, 81, 501-515.
8 J. Lee, S.-C. Lee, C. S. Hwang and J.-H. Choi, *Journal of Materials Chemistry C*, 2013, 1, 6364-6374.
9 Y. S. Jung, J. Y. Seo, D. W. Lee and D. Y. Jeon, *Thin Solid Films* 2003, 445, 63-71.
10 S.-J. Seo, C. G. Choi, Y. H. Hwang and B.-S. Bae, *J. Phys. D: Appl. Phys.* , 2009, 42, 035106.
11 K. Nomura, H. Ohta, A. Takagi, T. Kamiya, M. Hirano and H. Hosono, *Nature*, 2004, 432, 488-492.
12 J. E. Medvedeva and C. L. Hettiarachchi, *Phys. Rev. B*, 2010, 81, 125116.
13 A. Dolgonos, K. Lam, K. R. Poeppelmeier, A. J. Freeman and T. O. Mason, *J. Appl. Phys.* , 2014, 115, 013703.
14 D.-Y. Cho, J. Song, K. D. Na, C. S. Hwang, J. H. Jeong, J. K. Jeong and Y.-G. Mo, *Appl. Phys. Lett.* , 2009, 94, 112112.
15 L. Bizo, J. Choisnet, R. Retoux and B. Raveau, *Solid State Commun.* , 2005, 136, 163-168.
16 D. R. Kammler, T. O. Mason and K. R. Poeppelmeier, *J. Am. Ceram. Soc.* , 2001, 84, 1004-1009.
17 D. R. Kammler, T. O. Mason and K. R. Poeppelmeier, *Chem. Mater.* , 2000, 12, 1954-1960.
18 J. Ni, L. Wang, Y. Yang, H. Yan, S. Jin, T. J. Marks, J. R. Ireland and C. R. Kannewurf, *Inorg. Chem.* , 2005, 44, 6071-6076.
19 D. Bérardan, E. Guilmeau, A. Maignan and B. Raveau, *J. Appl. Phys.* , 2008, 104, 064918.
20 L. Bizo, J. Choisnet and B. Raveau, *Mater. Res. Bull.* , 2006, 41, 2232-2237.
21 D.-J. Lee, J.-Y. Kwon, J. Kim, K.-J. Kim, Y.-H. Cho, S.-Y. Cho, S.-H. Kim, J. Xu and K.-B. Kim, *J. Phys. Chem. C*, 2014, 118, 408-415.
22 D. B. Buchholz, J. Liu, T. J. Marks, M. Zhang and R. P. Chang, *ACS Appl Mater Interfaces*, 2009, 1, 2147-2153.
23 A. Walsh, J. L. F. Da Silva and S.-H. Wei, *Chem. Mater.* , 2009, 21, 5119-5124.
24 C. A. Hoel, J. M. G. Amores, E. Morán, M. A. Álario-Franco, J.-F. Gaillard and K. R. Poeppelmeier, *J. Am. Chem. Soc.* , 2010, 132, 16479-16487.
25 M.-G. Kim, H. S. Kim, Y.-G. Ha, J. He, M. G. Kanatzidis, A. Facchetti and T. J. Marks, *J. Am. Chem. Soc.* , 2010, 132, 10352-10364.
26 Damisih, H. C. Ma, J.-J. Kim and H. Y. Lee, *Thin Solid Films* 2012, 520, 3741-3745.
27 C. A. Hoel, T. O. Mason, J.-F. o. Gaillard and K. R. Poeppelmeier, *Chem. Mater.* , 2010, 22, 3569-3579.
28 S. H. Kwon, Y. M. Kang, Y. R. Cho, S. H. Kim and P. K. Song, *Surf. Coat. Technol.* , 2010, 205, S312-S317.
29 G.-S. Heo, Y. Matsumoto, I.-G. Gim, J.-W. Park, K.-Y. Kim and T.-W. Kim, *Solid State Commun.* , 2009, 149, 1731-1734.
30 S. h. Kwon, J. h. Jung, W. s. Cheong, G. h. Lee and P. k. Song, *Curr. Appl Phys.* , 2012, 12, S59-S63.
31 Cathleen A. Hoel, S. Xie, C. Benmore, Christos D. Malliakas, J.-F. Gaillard and Kenneth R. Poeppelmeier, *Z. Anorg. Allg. Chem.* , 2011, 637, 885-894.
32 S. P. Harvey, T. O. Mason, C. Korber and A. Klein, *Phys. Chem. Chem. Phys.* , 2009, 11, 3099-3104.
33 C. W. Ow-Yang, H.-y. Yeom and D. C. Paine, *Thin Solid Films* 2008, 516, 3105-3111.
34 A. Ambrosini, S. Malo, K. R. Poeppelmeier, M. A. Lane, C. R. Kannewurf and T. O. Mason, *Chem. Mater.* , 2002, 14, 58-63.
35 G. B. Palmer, K. R. Poeppelmeier and T. O. Mason, *Chem. Mater.* , 1997, 9, 3121-3126.
36 C. A. Hoel, J.-F. Gaillard and K. R. Poeppelmeier, *J. Solid State Chem.* , 2010, 183, 761-768.
37 S. P. Harvey, T. O. Mason, D. B. Buchholz, R. P. H. Chang, C. Körber and A. Klein, *J. Am. Ceram. Soc.* , 2008, 91, 467-472.
38 G.-S. Heo, I.-G. Gim, J.-W. Park, K.-Y. Kim and T.-W. Kim, *J. Solid State Chem.* , 2009, 182, 2937-2940.
39 K. J. Chen, F. Y. Hung, S. J. Chang, J. D. Liao, C. C. Weng and Z. S. Hu, *Appl. Surf. Sci.* , 2011, 258, 1157-1163.
40 J. M. Phillips, R. J. Cava, G. A. Thomas, S. A. Carter, J. Kwo, T. Siegrist, J. J. Krajewski, J. H. Marshall, W. F. Peck and D. H. Rapkine, *Appl. Phys. Lett.* , 1995, 67, 2246.
41 K. J. Chen, F. Y. Hung, S. J. Chang, S. J. Young, Z. S. Hu and S. P. Chang, *J. Sol-Gel Sci. Technol.* , 2010, 54, 347-354.

Journal of Materials Chemistry C Accepted Manuscript

This journal is © The Royal Society of Chemistry 20xx

42 Y. R. Denny, K. Lee, S. Seo, S. K. Oh, H. J. Kang, D. S. Yang, S. Heo, J. G. Chung and J. C. Lee, *Appl. Surf. Sci.* , 2014, 315, 454-458.
43 M. Putri, C. Y. Koo, J.-A. Lee, J.-J. Kim and H. Y. Lee, *Thin Solid Films* 2014, 559, 44-48.
44 J.-Y. Noh, H. Kim, H.-H. Nahm, Y.-S. Kim, D. Hwan Kim, B.-D. Ahn, J.-H. Lim, G. Hee Kim, J.-H. Lee and J. Song, *J. Appl. Phys.* , 2013, 113, 183706.
45 J. Ni, H. Yan, A. Wang, Y. Yang, C. L. Stern, A. W. Metz, S. Jin, L. Wang, T. J. Marks, J. R. Ireland and C. R. Kannewurf, *J. Am. Chem. Soc.* , 2005, 127, 5613-5624.
46 C. A. Hoel, D. B. Buchholz, R. P. H. Chang and K. R. Poeppelmeier, *Thin Solid Films* 2012, 520, 2938-2942.
47 B. Yaglioglu, H.-Y. Yeom and D. C. Paine, *Appl. Phys. Lett.* , 2005, 86, 261908.
48 K. Yong-Min, *J. Korean. Phys. Soc.*, 2009, 55, 1901.
49 A. Ambrosini, G. B. Palmer, A. Maignan, K. R. Poeppelmeier, M. A. Lane, P. Brazis, C. R. Kannewurf, T. Hogan and T. O. Mason, *Chem. Mater.* , 2002, 14, 52-57.
50 Y. Zhu, R. J. Mendelsberg, J. Zhu, J. Han and A. Anders, *J. Phys. D: Appl. Phys.* , 2013, 46, 195102.
51 P. D. C. King and T. D. Veal, *J. Phys.: Condens. Matter* 2011, 23, 334214.
52 D. E. Proffit, Q. Ma, D. B. Buchholz, R. P. H. Chang, M. J. Bedzyk, T. O. Mason and N. J. Dudney, *J. Am. Ceram. Soc.* , 2012, 95, 3657-3664.
53 G. Kresse and J. Furthmüller, *Comput. Mater. Sci.* , 1996, 6, 15-50.
54 G. Kresse and J. Furthmüller, *Phys. Rev. B*, 1996, 54, 11169-11186.
55 G. Kresse and D. Joubert, *Phys. Rev. B*, 1999, 59, 1758-1775.
56 V. I. Anisimov, J. Zaanen and O. K. Andersen, *Phys. Rev. B*, 1991, 44, 943-912.
57 P. Erhart, A. Klein, R. Egdell and K. Albe, *Phys. Rev. B*, 2007, 75, 153205.
58 H.-H. Nahm and Y.-S. Kim, *Appl. Phys. Lett.* , 2013, 102, 152101.
59 59.Y.-B. Lu, Y. Dai, M. Guo, L. Yu and B. B. Huang, *Phys. Chem. Chem. Phys.* , 2013, 15, 5208-5214.
60 P. E. Blochl, *Phys. Rev. B*, 1994, 50, 17953-17979.
61 C. G. Van de Walle and J. Neugebauer, *J. Appl. Phys.* , 2004, 95, 3851-3879.
62 O. Mryasov and A. Freeman, *Phys. Rev. B*, 2001, 64, 233111.
63 Y.-B. Lu, Y. Dai, W. Wei, Y. T. Zhu and B. B. Huang, *ChemPhysChem*, 2013, 14, 3916-3924.
64 J. Zhu, F. Liu, G. B. Stringfellow and S.-H. Wei, *Phys. Rev. Lett.* , 2010, 105, 195503.
65 W. Wei, Y. Dai, M. Guo, L. Yu, H. Jin, S. H. Han and B. B. Huang, *Phys. Chem. Chem. Phys.* , 2010, 12, 7612-7619.
66 B. Puchala and D. Morgan, *Phys. Rev. B*, 2012, 85, 195207.
67 S. Limpijumnong, S. Zhang, S.-H. Wei and C. Park, *Phys. Rev. Lett.* , 2004, 92, 155504.
68 L. Wang and A. Zunger, *Phys. Rev. B*, 2002, 66, 161202(R).
69 A. Janotti and C. G. Van de Walle, *Phys. Rev. B*, 2007, 76, 165202.
70 L. S. Vlasenko and G. D. Watkins, *Phys. Rev. B*, 2005, 72, 035203.
71 D. E. Proffit, D. B. Buchholz, R. P. H. Chang, M. J. Bedzyk, T. O. Mason and Q. Ma, *J. Appl. Phys.* , 2009, 106, 113524.
72 P. Agoston, P. Erhart, A. Klein and K. Albe, *J Phys Condens Matter*, 2009, 21, 455801.
73 D.-S. Liu, C.-H. Lin, F.-C. Tsai and C.-C. Wu, *Journal of Vacuum Science & Technology A*, 2006, 24, 694-699.
74 S. Z. Karazhanov, P. Ravindran, P. Vajeeston, A. Ulyashin, T. G. Finstad and H. Fjellvåg, *Phys. Rev. B*, 2007, 76, 075129.
75 K. S. Yang, Y. Dai and B. B. Huang, *Phys. Rev. B*, 2007, 76, 195201.

Journal of Materials Chemistry C Accepted Manuscript

Please do not adjust margins

Journal of Materials Chemistry C

ARTICLE

Table of content entry.

In multicomponent TCOs of In-Zn-Sn Oxide, the modulation of constituent elements on carrier generation and charge transport are interpreted.

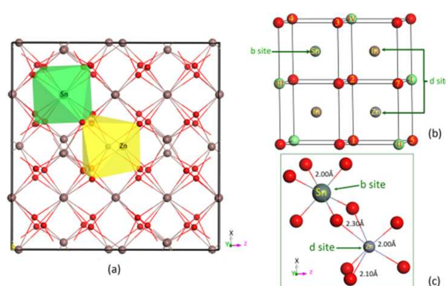

Journal of Materials Chemistry C Accepted Manuscript

Please do not adjust margins